



UNIVERSITY OF LEEDS

This is a repository copy of *Pom-pom-like constitutive equations for comb polymers*.

White Rose Research Online URL for this paper:

<http://eprints.whiterose.ac.uk/81230/>

Version: Accepted Version

Article:

Lentzakis, H, Das, C, Vlassopoulos, D et al. (1 more author) (2014) Pom-pom-like constitutive equations for comb polymers. *Journal of Rheology*, 58 (6). 1855 - 1875. ISSN 0148-6055

<https://doi.org/10.1122/1.4895606>

Reuse

Unless indicated otherwise, fulltext items are protected by copyright with all rights reserved. The copyright exception in section 29 of the Copyright, Designs and Patents Act 1988 allows the making of a single copy solely for the purpose of non-commercial research or private study within the limits of fair dealing. The publisher or other rights-holder may allow further reproduction and re-use of this version - refer to the White Rose Research Online record for this item. Where records identify the publisher as the copyright holder, users can verify any specific terms of use on the publisher's website.

Takedown

If you consider content in White Rose Research Online to be in breach of UK law, please notify us by emailing eprints@whiterose.ac.uk including the URL of the record and the reason for the withdrawal request.



eprints@whiterose.ac.uk
<https://eprints.whiterose.ac.uk/>

Pom-pom like constitutive equations for comb polymers

Helen Lentzakis,^{1, 2, a)} Chinmay Das,^{3, b)} Dimitris Vlassopoulos,^{1, 2, c)} and Daniel J. Read^{3, d)}

¹⁾*Foundation for Research and Technology Hellas (FORTH),
Institute of Electronic Structure & Laser, Heraklion, Crete 71110,
Greece*

²⁾*Department of Materials Science & Technology, University of Crete, Heraklion,
Crete 71300, Greece*

³⁾*School of Mathematics, University of Leeds, Leeds, LS2 9JT,
U.K.*

(Dated: 31 August 2014)

In analogy with the pom-pom model, we introduce a simple model for comb polymers with multiple side-arms attached to a linear backbone by considering a set of coupled equations describing the stretch in the individual inter-branch backbone segments. The stretch equations predict a sudden onset of backbone stretch as the flow rate is increased. Drag-strain coupling smooths this transition to some extent. For a series of well characterized polyisoprene and polystyrene combs, we find good agreement with the experimentally determined transient stress growth coefficients in uniaxial extension.

^{a)}Electronic mail: helen.lentzakis@espci.fr; Current Address: Matière Molle et Chimie, ESPCI ParisTech, 10 Rue Vauquelin, 75005 Paris, France

^{b)}Electronic mail: c.das@leeds.ac.uk

^{c)}Electronic mail: dvlasso@iesl.forth.gr

^{d)}Electronic mail: d.j.read@leeds.ac.uk

I. INTRODUCTION

Understanding and predicting the rheological consequences of molecular structure in entangled branched polymers remains a formidable challenge with scientific and technological implications. Compared to linear entangled polymers, long-chain branching exhibits distinct linear and nonlinear viscoelastic response, characterized by hierarchical relaxation, weaker shear thinning with faster onset and strain hardening at low rates [Mendelson, Bowles, and Finger, 1970; Samurkas, Dealy, and Larson, 1989; Wood-Adams *et al.*, 2000; Hatzikiriakos, 2000; Kasehagen and Macosko, 1998; Dealy and Larson, 2006; Das *et al.*, 2006a; McLeish, 2008; Read *et al.*, 2011]. These phenomena play a key role in the processing of commercial polymers. It is desirable to achieve full control of industrial processes and eventually design *in silico* specific classes of branched polymers with desired properties for given applications. To this end, it is important to understand the molecular origin of different rheological phenomena [Read *et al.*, 2011].

To accomplish this ambitious task, it is important to use model, well-characterized polymers and mesoscopic modeling. Significant advances have been made in both fronts. Concerning the former, branched polymers with controlled structure can be obtained via high-vacuum anionic synthesis and thorough characterization often involving combination of Size Exclusion Chromatography with Temperature Gradient Interaction Chromatography [Chambon *et al.*, 2008; Li *et al.*, 2010; Chen *et al.*, 2011; Snijkers *et al.*, 2011; Hutchings *et al.*, 2012]. On the other hand, the linear viscoelasticity of model branched polymers is well described by invoking the different relaxation mechanisms (reptation, contour length fluctuations, dynamic tube dilution) and the concept of hierarchical relaxation (outer branches relax first, inner branches follow) in the tube model [Doi and Edwards, 1986; Ball and McLeish, 1989; Milner and McLeish, 1997; McLeish, 2002]. Accurate, parameter-free predictions encompass a range of complex molecular structures including H-polymers, combs, pom-pom polymers and Cayley trees [McLeish and Larson, 1998; Blackwell, Harlen, and McLeish, 2001; Kapnistos *et al.*, 2005; Inkson *et al.*, 2006; Van Ruymbeke *et al.*, 2010; Ahmadi *et al.*, 2011]. This predictive toolbox was generalized for random branching (which is relevant to commercial polymers) and led to the development of the Hierarchical model [Larson, 2001; Larson *et al.*, 2007] and the BoB algorithm [Das *et al.*, 2006a]. Of particular mention is the latest development with BoB where the polymerization reactions were incor-

porated and linked to structure via a stochastic approach, hence also linking polymerization to flow properties [Read *et al.*, 2011; Das *et al.*, 2014].

Despite these significant advances, modeling nonlinear rheology is less developed. Important contributions at different level of coarse graining include the pom-pom model [McLeish and Larson, 1998] and the molecular-stress function (MSF) approach [Wagner and Rolón-Garrido, 2008; Rolón-Garrido *et al.*, 2009]. Interestingly, these models are highly successful in predicting data with ill-defined commercial polyethylenes. In this respect, we note BoB's ability to do so as well [Read *et al.*, 2011; Das *et al.*, 2014]. However, linking molecular characteristics and nonlinear response in well-defined molecular structures remains an unresolved problem. The issue is that structures like pom-pom are relatively simple in the sense that a backbone has two branch points at its extremities. In such a case, the increased amount of chain stretch can be explained by the fact that the segment between two branch points is not free to relax its stress until the branches have fully retracted. Eventually, branch point withdrawal occurs since it becomes entropically favorable to withdraw branches instead of stretching further the backbone [McLeish and Larson, 1998]. Given this sound physical picture, the challenge is to generalize this case for multiple branch points along the backbone, where the stretch should propagate toward the center of the molecule.

Recently, attempts in this direction had been reported by using concepts of tube pressure in extension and the MSF [Nielsen *et al.*, 2006; Rolón-Garrido *et al.*, 2009]. However, the tube pressure has been recently criticized [Ianniruberto and Marrucci, 2012] as not providing a consistent description of hardening, for example in the case of linear polymer blends. Hence, building-up on the pom-pom ideas and developing molecular constitutive models for polymers with multiple branch points remains a formidable task, which we address in the present work.

The simplest class of molecules having multiple branch-points are comb polymers with a linear backbone and multiple side-arms. Comb polymers are not just of academic interest, because random synthesis techniques invariably produces mostly comb-like architectures when the branching probability is not too high [Das *et al.*, 2006a]. The main difference between the ideal combs to be considered in the present paper, and comb-like molecules produced via random synthesis, is that in the former the side arms are of relatively uniform length, whilst random synthesis usually produces side arms with a wide distribution of lengths. In addition, the side arms are randomly distributed along a backbone, also for ideal

combs.

For a comb polymer, while each of the backbone segments constrained between branch-points are capable of sustaining stretch, the maximum stretch that the different segments can sustain are different [Marrucci *et al.*, 2008; Snijkers *et al.*, 2013]. The connectivity along the molecule couples the evolution of the stretch in different backbone segments. This leads to a Rouse-like dynamics of the stretch evolution in flow.

The rest of the paper is organized as follows: In Sec. II we consider a comb molecule and develop the coupled equations that describe stretch evolution in flow. The comb is the simplest class of multiply-branched molecule, so a large number of rheological measurements already exist in the literature and we use previously published rheological data on a set of polyisoprene and polystyrene combs to compare predictions from our model (Sec. III). We conclude this paper with a discussion about how our model may be extended for more generic molecular topologies in Sec. IV.

II. GENERALIZED POM-POM STRETCH EQUATIONS FOR COMB POLYMERS

We consider a comb polymer with a linear backbone having Z_b entanglements (i.e. units of entanglement molar mass M_e) and assume that it is grafted uniformly with n_a side arms, each having Z_a entanglements. For the time being, we assume that n_a is odd ($n_a = 2n_s - 1$, where $2n_s$ is the number of backbone segments). In tube theory [Doi and Edwards, 1986], it is common to consider the averaged dynamics of the molecule, and in this approximation we can think of the central branch-point as the fixed origin about which the backbone stretches. Fig. 1 shows the numbering scheme of the branch-points and the contour lengths of the backbone segments. Since, both halves of the backbone about the central branch-point behave the same way, we only consider one half in the following. The assumption of uniform grafting ensures that all backbone segments between branch-points have the same equilibrium tube contour lengths l_{eq} .

At time-scales longer than the side-arm retraction time τ_a , the branch-points act like localized drag points. The friction coefficient ζ depends on the backbone tube diameter $a(t)$

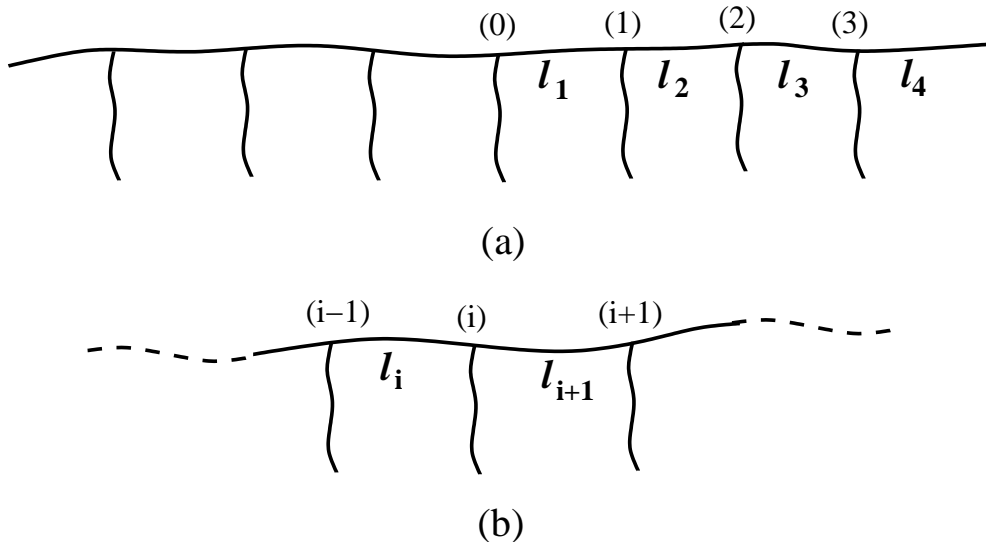


FIG. 1. (a) Cartoon of a seven arm comb polymer: We label branch-points starting from the center of the molecule. The equilibrium contour lengths of all the backbone segments between the branch-points are considered to be the same. In flow, the contour length of the backbone segment between the branch-points i and $i - 1$ is l_i . (b) The dynamics of the branch-point i is determined by the balance of the viscous force and the elastic force at i .

considered to describe the branch-point diffusion and is given by [Das *et al.*, 2006a]

$$\zeta(t) = \frac{2k_B T \tau_a}{p^2 a(\tau_a)^2} \left(\frac{a(t)}{a(\tau_a)} \right)^2. \quad (1)$$

Here, the parameter p describes the average hop size in units of the tube diameter $a(\tau_a)$ at the time scale τ_a . With the terminal relaxation time being τ_d (from eventual reptation of the molecules), for flow rates $\dot{\epsilon}$ between $1/\tau_d$ and $1/\tau_a$, only the backbone segments between branch-points are stretched. We determine the stretch of the segments from force balance at each branch-point. There are two forces to consider: the drag force due to the relative velocity of the branch-point with respect to the tube velocity, and the elastic force from the neighboring backbone segments.

Considering branch-point i (Fig. 1b), we define its curvilinear velocity along the tube axis, relative to the central branchpoint, to be v_i . The difference between v_i and the velocity of the surrounding tube matrix at the branch-point gives rise to a viscous force

$$f_v = -\zeta \left[v_i - (\mathbf{K} : \mathbf{S}) \sum_{j=1}^i l_j \right]. \quad (2)$$

Here, \mathbf{K} is the velocity gradient tensor, \mathbf{S} is the average tube orientation, and the contraction $\mathbf{K} : \mathbf{S}$ gives the fractional rate of increase in tube length. The segments l_{i+1} and l_i provide an elastic force

$$f_e = k(l_{i+1} - l_{eq}) - k(l_i - l_{eq}), \quad (3)$$

with k being the spring constant describing the Hookean elastic response of the backbone segments. From rubber-elasticity theory $k = 3k_B T / Z_s a^2$, with Z_s being the number of entanglements in one backbone segment between two branch-points. Setting $f_v + f_e = 0$, we find the branch-point velocity

$$\zeta v_i = k(l_{i+1} - l_i) + \zeta(\mathbf{K} : \mathbf{S}) \sum_{j=1}^i l_j. \quad (4)$$

The difference of velocity between the branch-points i and $i - 1$ gives the rate of change of the contour length of the segment between the two branch-points as

$$\begin{aligned} \zeta \frac{dl_i}{dt} &= \zeta(v_i - v_{i-1}) \\ &= k(l_{i+1} - 2l_i + l_{i-1}) + \zeta(\mathbf{K} : \mathbf{S}) l_i. \end{aligned} \quad (5)$$

Dividing by the equilibrium segment lengths l_{eq} and defining the dimensionless stretch $\lambda_i \equiv l_i / l_{eq}$ we arrive at

$$\frac{d\lambda_i}{dt} = \frac{1}{\tau_{seg,0}} (\lambda_{i+1} - 2\lambda_i + \lambda_{i-1}) + (\mathbf{K} : \mathbf{S}) \lambda_i. \quad (6)$$

Here, we defined the time $\tau_{seg,0} \equiv \zeta / k$ that determines stretch relaxation between backbone segments separated by branch-points. The outermost two segments on the backbone do not contribute to the stretch. Thus λ_{n_s} is always one.

We can approximately include the effect of local (\leq tube diameter a) displacement of branch-point from tension difference between the two sides of a branch-point, leading to so-called ‘‘drag-strain coupling’’ [Blackwell, McLeish, and Harlen, 2000]. For small displacements, considering the probability distribution of displacement to be Gaussian, the position of the branch-point can be considered as a Brownian walk in a quadratic potential [Doi and Edwards, 1986]. Balancing the force from this localizing potential to the elastic force at branch-point i , the effective contour length of the side-arm at i that participates in relaxation by retraction, is reduced by a factor proportional to $|\lambda_i - \lambda_{i+1}|$. Exponential dependence of the retraction time-scale on the side-arm length leads to an effectively shorter segmental stretch relaxation time from this drag-strain coupling as

$$\tau_{seg}(i) = \tau_{seg,0} \exp(-2|\lambda_i - \lambda_{i+1}|). \quad (7)$$

The factor 2 in the exponent of Eq. 7 deserves brief explanation. In the original work [Blackwell, McLeish, and Harlen, 2000] a factor $2/q$ appeared in the exponent of the drag strain coupling term, where q was the number of arms in the pom-pom. This factor was later corrected to $2/(q-1)$ (see e.g. [Hassell *et al.*, 2009] for possibly the earliest explicit mention of this correction). The reason, as explained in [McLeish, 2002], arises due to a quadratic interpolation of the effective retraction potential for the branchpoint, between its equilibrium position and a linear potential with slope proportional to $(q-1)$ at large depths of retraction. In the present case, the effective value of q is 2 (from three-functional branchpoints). So, for consistency with earlier work on drag-strain coupling, the factor $2/(q-1)$ appearing in the exponent is 2. Incorporating this drag-strain coupling, the equations for the stretch dynamics become

$$\frac{d\lambda_i}{dt} = \frac{1}{\tau_{seg,0}} [e^{2|\lambda_i - \lambda_{i+1}|} (\lambda_{i+1} - \lambda_i) - e^{2|\lambda_{i-1} - \lambda_i|} (\lambda_i - \lambda_{i-1})] + (\mathbf{K} : \mathbf{S}) \lambda_i. \quad (8)$$

For large deformations, it is possible that the stretch variable in adjacent backbone segments may differ by more than one, i.e. $|\lambda_i - \lambda_{i+1}| > 1$. A force balance argument, comparing the tension in the side arm and two backbone segments, indicates that such a situation is unsustainable, and “branchpoint withdrawal” occurs, in which the side arm is pulled into, and oriented along, the backbone tube (this type of force balance argument is equivalent to that made for branchpoint withdrawal in the pom-pom model [McLeish and Larson, 1998] and more generally when considering the “priority” variable in randomly branched polymers [Bick and McLeish, 1996; Read and McLeish, 2001]). The branch-point encounters a constant maximum force in such large deformation and hence an equivalent linear confining potential. In a general polymer, with different lengths of side arms, it might be that the conditions for branchpoint withdrawal are first fulfilled at internal segments along the backbone. In general, this could lead to quite complicated dynamics, since the resulting retraction of one backbone chain segment becomes a source of additional stretch of neighboring chain segments, possibly leading to internal cascades of branchpoint withdrawal. Fortunately in the present simple comb case, the dynamics are much more straightforward and branchpoint withdrawal occurs first from the outer segments, moving inwards through the molecule. In this case, it is sufficient, in the numerical implementation of the model, to ensure that the stretch λ_i in segment i is always less than or equal to $\lambda_{i+1} + 1$ [Inkson *et al.*, 1999; Blackwell, McLeish, and Harlen, 2000; Marrucci *et al.*, 2008]. For the present regular combs,

this ensures that the more general branch point withdrawal criterion of $|\lambda_i - \lambda_{i-1}| \leq 1$ is enforced. For irregular combs, more care would be required in numerical implementation of the model.

As with the original differential version of the pom-pom equations [McLeish and Larson, 1998], we determine the orientation tensor \mathbf{S} by working with an auxiliary tensor \mathbf{A} satisfying the upper convected Maxwell model [Bird, Armstrong, and Hassager, 1987]

$$\frac{\partial}{\partial t} \mathbf{A} = \mathbf{K} \cdot \mathbf{A} + \mathbf{A} \cdot \mathbf{K}^T - \frac{1}{\tau_o} (\mathbf{A} - \mathbf{I}), \quad (9)$$

with τ_o being the orientational relaxation time. The orientation tensor \mathbf{S} is given by

$$\mathbf{S}(t) = \frac{\mathbf{A}(t)}{\text{trace}[\mathbf{A}(t)]}. \quad (10)$$

For simplicity, we assume the orientation to be identical for all backbone segments on a given comb. In practice, this will not be exactly true and the outermost segments will be less oriented. However since the terminal relaxation of the comb is via reptation of the linear backbone, this mode dominates the orientation relaxation and most segments will have a similar orientation, i.e. the approximation is not such a bad one. A possible extension of the model would be to allow different backbone segments to relax orientation at different rates.

The total stress for a comb in a nonlinear flow is found by summing over the contributions from stretched backbone segments, and is given by

$$\sigma(t) = \frac{3g}{n_s - 1} \sum_{i=1}^{n_s-1} \lambda_i^2(t) \mathbf{S}(t). \quad (11)$$

Here, from the assumption of uniform grafting, we consider each segment of the backbone contributes equally to the modulus g .

Having defined the constitutive model for a single comb, we wish to make comparison with experiments on real comb samples. In the spirit of the multimode version of the original pom-pom model, we describe that the linear viscoelasticity of the comb molecules with a set of n_M Maxwell modes, such that the α -th mode is characterized by a modulus g_α and a relaxation time $\tau_{o,\alpha}$. Note that the linear data are well described by hierarchical tube modeling [Kapnistos *et al.*, 2005; Kirkwood *et al.*, 2009]. The modes with the fastest relaxation times correspond to stress contributions from the side-arms (and the outermost of the backbone). We model the nonlinear response of these modes using the non-stretching version

of the pom-pom model. The slowest modes correspond to comb-backbone relaxations, and (for simplicity) we model the nonlinear response for *each* of these modes using a separate instance of the above comb model. We detail below our criterion for assigning a given mode to be comb or non-stretching. Assuming there are k_N non-stretching modes, and $n_M - k_N$ comb modes, the total stress is obtained from

$$\sigma = 3 \sum_{\alpha=1}^{k_N} g_{\alpha} \mathbf{S}_{\alpha}(t) + \frac{3}{n_s - 1} \sum_{\alpha=k_N+1}^{n_M} \sum_{i=1}^{n_s-1} g_{\alpha} \lambda_{i,\alpha}^2(t) \mathbf{S}_{\alpha}(t). \quad (12)$$

Here, $\mathbf{S}_{\alpha}(t)$ is average tube orientation experienced by the fraction that contributes to the α -th Maxwell mode evaluated from Eqns. 9 and 10 with the orientational relaxation time as $\tau_{o,\alpha}$. For the comb modes, we consider equal contribution to the modulus from each of the internal segments of the backbone with $\lambda_{i,\alpha}$ being the stretch on the i -th backbone segment that contributes to the α -th Maxwell mode.

III. COMPARISONS WITH EXPERIMENTS

To compare with our model predictions, we use published experimental data on a set of well-characterized and well-studied anionically synthesized polyisoprene (PI) [Kirkwood *et al.*, 2009] and polystyrene (PS) [Roovers, 1979] combs. These set of combs have been studied by multiple authors concentrating on different flow experiments. Roovers and Graessley [1981] studied the linear viscoelastic properties of the PS combs. Kapnistos *et al.* [2005] revisited and extended the linear viscoelastic measurements and developed an analytical model for linear relaxation in comb polymers. Kapnistos *et al.* [2009] looked at the nonlinear response after large step strain in a subset of the PS combs at different dilution. Kirkwood *et al.* [2009] measured the stress response in both small angle oscillatory shear and in nonlinear step strain for the PI combs with short (unentangled to barely entangled) side arms. Most recently Lentzakis *et al.* [2013] used both the PS and PI combs to measure the uniaxial extensional response. Lentzakis *et al.* [2013] also reported gel-permeation chromatography to confirm the stability of the molecules since synthesis, and, temperature-gradient interaction chromatography to confirm the narrow distribution of the combs. We use the data set from [Lentzakis *et al.*, 2013] to compare with our theoretical modeling. Table I summarizes the molecular architecture of the comb polymers used in this work.

Briefly, the extensional rheology measurements were performed at 170°C for the polystyrene

| Sample | M_b (kg/mol) | M_a (kg/mol) | n_a | $\tau_a^{(a)}$ (s) | $\tau_{seg,0}^{(b)}$ (s) | $\tau_{seg,0}^{(c)}$ (s) |
|--------|-------------------|-------------------|-------|-----------------------|-----------------------------|-----------------------------|
| PI211 | 157 | 6.3 | 8.6 | 0.003 | 0.25 | 0.22 |
| PI254 | 120.5 | 18.8 | 7.1 | 0.9 | 20 | 28 |
| PI472 | 370 | 5.8 | 17.6 | 0.003 | 0.45 | 0.3 |
| PS622 | 275 | 11.7 | 30 | 0.013 | 0.04 | 0.09 |
| PS642 | 275 | 47 | 29 | 2.2 | 1.0 | 4.6 |
| PS712 | 860 | 6.5 | 30 | 0.0016 | 0.025 | 0.07 |
| PS722 | 860 | 11.7 | 28 | 0.0029 | 0.12 | 0.12 |
| PS732 | 860 | 25.7 | 26 | 0.04 | 0.90 | 1.4 |
| PS742 | 860 | 47 | 29 | 0.7 | 20.0 | 14.3 |

TABLE I. Molecular characteristics of the combs used in this work. The backbone molar mass M_b , side-arm molar mass M_a , and the number of side-arm n_a for the PI combs are from [Kirkwood *et al.*, 2009] and the PS combs from [Roovers, 1979]. ^(a) Side-arm retraction time estimated from the phase angle. ^(b) Values used for the segmental stretch relaxation times to fit the experimental data with our model. ^(c) Estimates from Eqn. 13.

combs and at 0°C for the polyisoprene combs using an SER fixture [Sentmanat, 2004] mounted on an ARES 2KFRTN1 strain-controlled rheometer (TA, USA). Due to the limitations inherent in SER, experiments are limited to a maximum Hencky strain of 4, and a steady-state tensile growth coefficient could not be unambiguously determined. Therefore, the modeled data can only be compared to the experimental data in a limited Hencky strain range. On the other hand, a wide range of extensional rates (especially in the high-rate limit) was obtained [Lentzakis *et al.*, 2013].

In applying our model, we start by fitting the linear viscoelastic moduli measured from small amplitude oscillatory shear (SAOS) with approximately three Maxwell modes per decade in frequency range of the experimental data. The Maxwell times were chosen to be uniform in log-scale. We use a least-square fit to the viscous and elastic responses along with a regularization term [Press *et al.*, 1992] to ensure that all g_M are positive and $g_M(t_M)$ are smooth (Appendix A details the fitting procedure). For combs with long side-arms, the

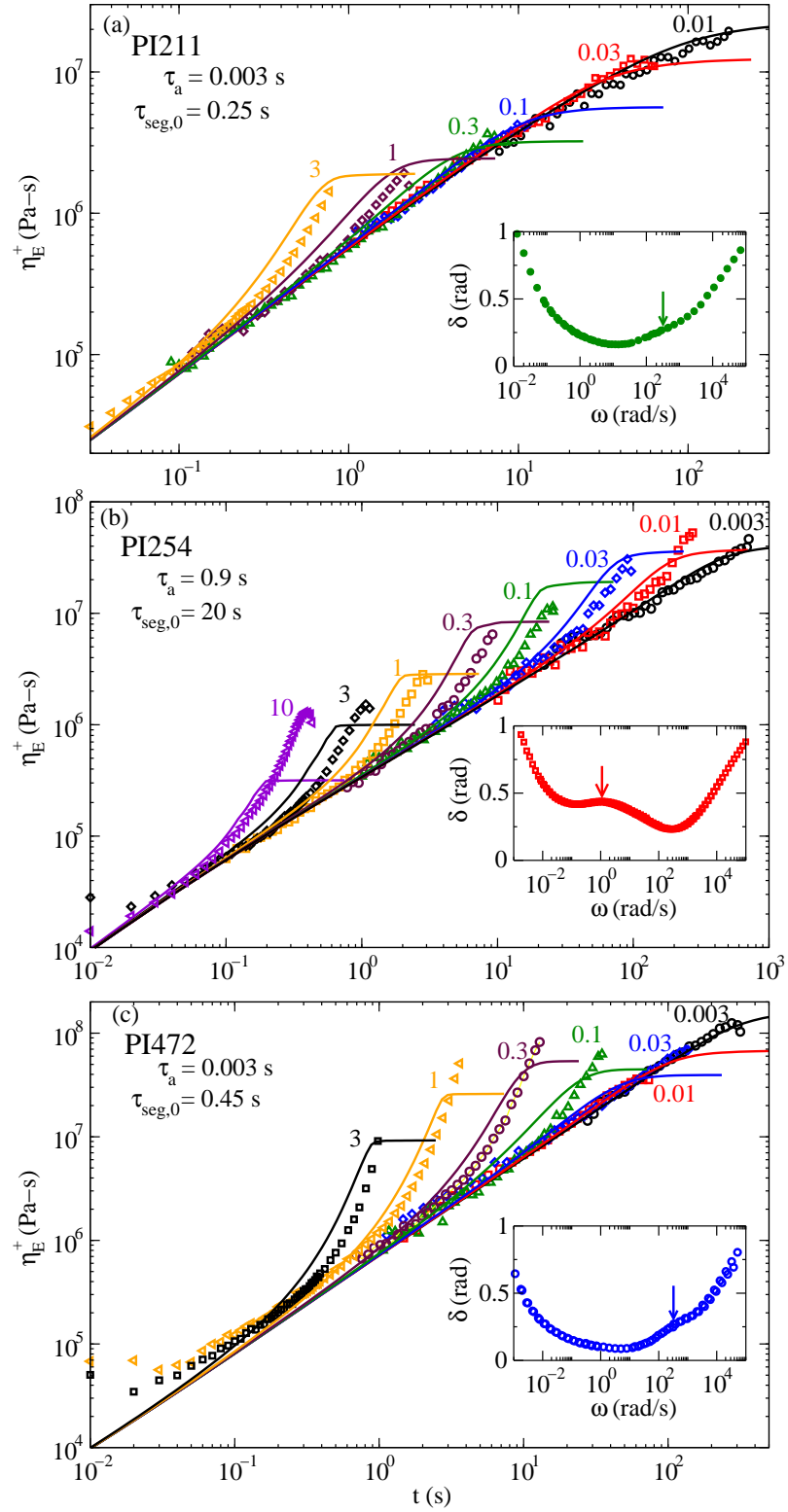


FIG. 2. Experimental data (symbols) and model predictions for the start-up stress growth coefficients in extensional flow at the indicated rates for the PI combs. Insets show the phase angle with arrows indicating frequency that determines τ_a .

phase angle (δ) shows a distinct peak in the time-scale of arm retraction τ_a in the SAOS data. When the side-arms are not long enough, there is a change of slope in the phase angle. For each of the experimental resins, we select τ_a from the peak/point of change in slope in the phase angle. We expect these estimates for τ_a to have large uncertainty (up to a factor 2) [Bačová *et al.*, 2014].

Though the side-arms and the backbones in the resins have very small polydispersity, the synthesis procedure places the side-arms at random positions on the backbone and the number of side-arms vary between molecules [Chambon *et al.*, 2008; Lentzakis *et al.*, 2013]. However, with a large number of side-arms, as in the present case, the distribution of number of arms is sharp about the mean. Consideration of an uniform comb with average number of side-arms placed with uniform spacing provides reasonably good description of the architecturally polydisperse resin [Chambon *et al.*, 2008]. We consider this idealized uniform comb with regular spacing and the number of side-arm set to the nearest odd integer to the experimentally determined average number of arms to apply our model. This is likely to provide a good description in the present case with large number of side-arms. But more detailed analysis that captures this architectural polydispersity probably will be needed to describe combs with only a few side-arms. Because of the distribution of inter-branch segment lengths, at intermediate extension rates, locally it is possible for the order of arm retraction to deviate from strict "outside first" scenario considered here. However, with the large number of side-arms, globally the picture of branch-point withdrawal proceeding generally from outside to the center of the molecule will remain valid (i.e. typically branch-points towards the outside of the molecule retract before those on the inside, even if the precise order is not monotonically from the outside to the inside). In this sense our model captures the "average" behavior.

As noted above, we require a criterion to decide which of the Maxwell modes are to be assigned as stretching, or comb-modes, in Eqn. 12. We treat the Maxwell modes with relaxation times faster than the arm retraction time ($\tau_{o,\alpha} < \tau_a$) as non-stretching ($\lambda_i = 1$ for all i). All slower modes are treated as comb-modes. We also tested alternative criteria for assigning the modes. For example, one can estimate the shear modulus associated with entangled comb backbones after the side arms have relaxed; one then assigns, as "comb-modes", the slowest Maxwell modes such that their total shear modulus amounts to the estimated modulus of the diluted backbones. The final results for the predicted start-up

stress growth coefficients (transient viscosity η_E^+) are not strongly sensitive to the chosen criterion.

The time-scales of the Maxwell modes define the orientation relaxation times of the modes. We keep the segmental stretch relaxation time $\tau_{seg,0}$ as a global fitting parameter (i.e. we use the same value of $\tau_{seg,0}$ for all comb modes for a given resin). We use the analytically known solution for \mathbf{A} in uniaxial extension and numerically solve the coupled stretch equations (Eqn. 8) by using a fifth order Cash-Karp Runge-Kutta method with adaptive step-size [Press *et al.*, 1992].

Figs. 2-4 show the experimental data (symbols) and model predictions (lines) for the start-up stress growth coefficients in uniaxial extension for combs at a number of extension rates. Insets in the plots show the phase angle with arrows pointing the angular frequency that determines τ_a . For each of the combs, we varied $\tau_{seg,0}$ to best fit the data giving particular attention to the rate at which strain-hardening shows-up for the first time.

For PS642 (Fig. 3b), we show predictions with $\tau_a = 2.2$ s (solid lines) and $\tau_a = 1.25$ s. In our calculations, decreasing τ_a results in assigning more modes as stretching modes. This results in increased stress with decreasing τ_a for rates comparable or more than $1/\tau_a$. Note that τ_a for most of the resins considered are much lower than that of PS642. Thus, most of the resins considered here show little dependence on the exact value of τ_a used.

Where the experimental rates span the onset of strain hardening (PI211, PI472, PS712, PS722, and PS732) only values of $\tau_{seg,0}$ in a limited range describes the data well. For PS712 (Fig. 3c), we show predictions with $\tau_{seg,0} = 0.025$ s (solid lines) and $\tau_{seg,0} = 0.07$ s (dashed lines). The solid lines show an onset of strain hardening at $\dot{\epsilon} = 0.3$ /s consistent with the experimental data. The dashed lines show the onset at a lower rate ($\dot{\epsilon} = 0.1$ /s. While the stress is sensitive to $\tau_{seg,0}$ at rates close to the onset of strain hardening, the stress does not depend on $\tau_{seg,0}$ either at rates much higher than this critical rate (where all the backbone segments are maximally stretched) or at rates much lower than this critical rate (where none of the backbone segments are stretched).

The present experiments with the SER fixture cannot unambiguously suggest the occurrence of maximum extensional viscosity or steady state values. But the predictions from the model are in reasonably good agreement with the data given its crude assumptions. The highest experimental rates are comparable to the inverse of the bare Rouse time of the molecules [Lentzakis *et al.*, 2013] and we are likely to underestimate the stress there.

At such rates there is not sufficient time for branchpoint withdrawal; chains then stretch beyond the limit normally set by branchpoint withdrawal. We consistently underpredict the stress for PI472 (Fig. 2c) for all rates that show strain hardening. It is possible to improve the predictions for the maximum of η_E^+ to some extent by increasing $\tau_{seg,0}$ and decreasing τ_a . However, such change of parameters also change the rate at which strain hardening shows up for the first time.

Assuming, in Eqn. 1, that the relevant tube diameter for both the branch-point friction and the stress relaxation is the backbone tube diameter at the end of side-arm retraction, $a(\tau_a)$, we can estimate $\tau_{seg,0}$ as

$$\tau_{seg,0} \simeq \frac{2}{3} \frac{Z_s \tau_a}{p^2} \phi_{bb}^\alpha, \quad (13)$$

where $\phi_{bb} \simeq (Z_b - 2Z_a)/(Z_b + n_a Z_a)$ is the weight fraction of backbone material, and α is the dilution exponent. We estimate Z_s as $Z_s \simeq Z_b/(n_a + 1)$. In Table I, we show values of $\tau_{seg,0}$ used in the fitting procedure and estimated from Eq. 13 assuming $\alpha = 1$, $M_e(PI) = 4.1 \text{ kg/mol}$, $M_e(PS) = 12.9 \text{ kg/mol}$, and $p^2 = 1/40$. Note that the definition of M_e used here includes a $(4/5)$ prefactor [Fetters *et al.*, 1994; Kapnistos *et al.*, 2005; Kirkwood *et al.*, 2009]. The values of α and p^2 used here were found to describe the linear relaxation of a number of different resins with different level of branching and with different chemistries [Das *et al.*, 2006a,b; Chambon *et al.*, 2008; Read *et al.*, 2011; Hutchings *et al.*, 2012]. Our estimates for τ_a from visual inspection of the phase angle could give an error of a factor 2 [Bačová *et al.*, 2014]. We use a single segment length Z_s ; though the synthesis procedure should create a wide distribution of Z_s . The value of p^2 can be different by a factor of 2 from the value used here and may depend on the architecture/chemistry [Bačová *et al.*, 2014]. Considering these uncertainties, the agreements between the fit values and the estimates from Eq. 13 are satisfying. This is even more remarkable (and perhaps surprising) because some of the PS combs have barely entangled side-arms with inter-branch point backbone sections that are shorter than the entanglement molecular weight. With respect to the comb polymers with unentangled side branches, it is worth brief further comment. Whilst our model was developed for entangled side branches, it is to be expected that it is possible to match some aspects of data for the unentangled side-arm cases. In the absence of branch-point withdrawal (i.e. for small stretches), the stretch dynamics given by Eqn. 6 are effectively a discrete version of a Rouse-chain in a tube, and could equally well describe the extensional rheology of a linear polymer (i.e. a comb with zero length arms) - the onset

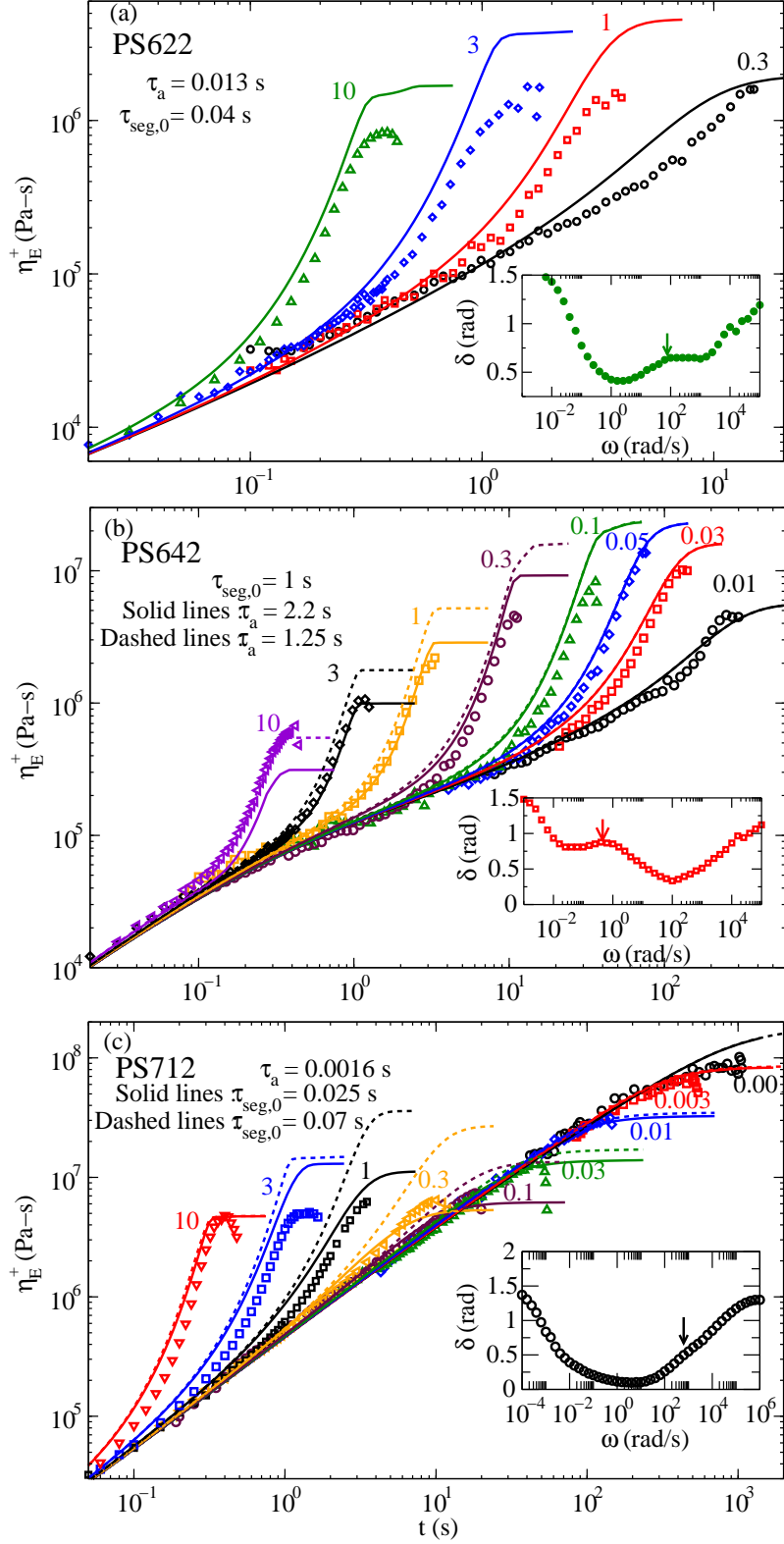


FIG. 3. Experimental data (symbols) and model predictions for the start-up stress growth coefficients in extensional flow at the indicated rates for (a) PS622, (b) PS642, and (c) PS712. Insets show the phase angle with arrows indicating frequency that determines τ_a .

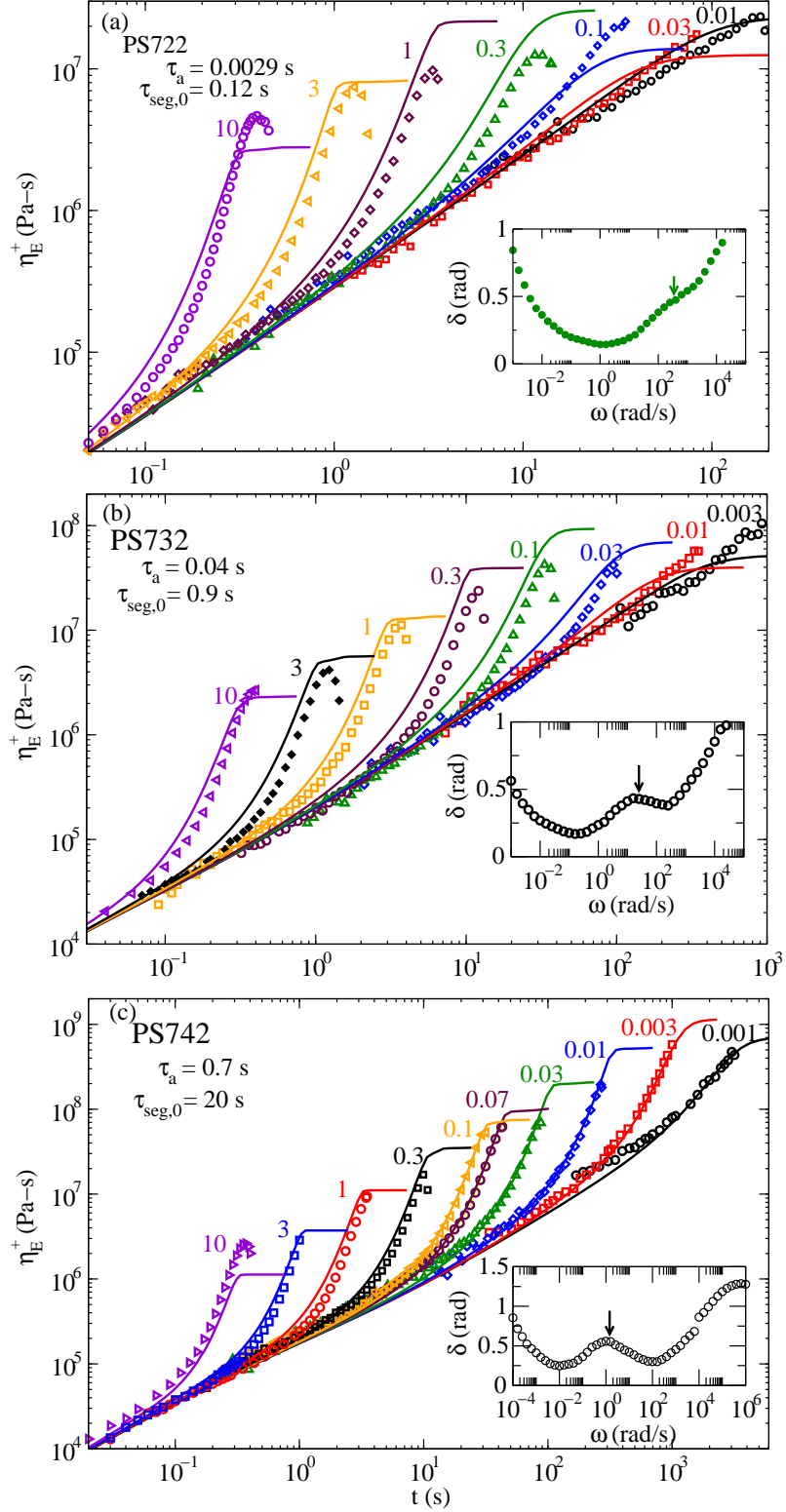


FIG. 4. Experimental data (symbols) and model predictions for the start-up stress growth coefficients in extensional flow at the indicated rates for (a) PS722, (b) PS732, and (c) PS742. Insets show the phase angle with arrows indicating frequency that determines τ_a .

rate for extension hardening is simply the inverse of the Rouse time. For this reason we would expect to be able to model the onset of extension hardening at low strains. However, for unentangled branches, we would not expect branchpoint withdrawal to play a role. For reasons still not completely understood, experimentally short side-branches seem to provide larger friction than predicted from star-arm retraction theory [Zhou and Larson, 2007; van Ruymbeke *et al.*, 2007; Kirkwood *et al.*, 2009]. This has been often modeled by artificially increasing the length of the side-arm in theoretical calculations. The fact that our estimated timescales from Eqn. 13 are at all close to the fit values, and that the predicted extent of extension hardening is at approximately the correct level, suggests that tube-based models continue to provide reasonable description even when side-arms are barely entangled (with some modifications like artificially increasing the length of the side-arms or as in the present case by treating $\tau_{seg,0}$ as a fitting parameter). Of course, we cannot rule out the possibility that the apparent agreement, even for the combs with barely entangled side-arms, is a coincidence. We note, that beyond the time-scale of arm retraction, the backbones remain well-entangled for all the resins.

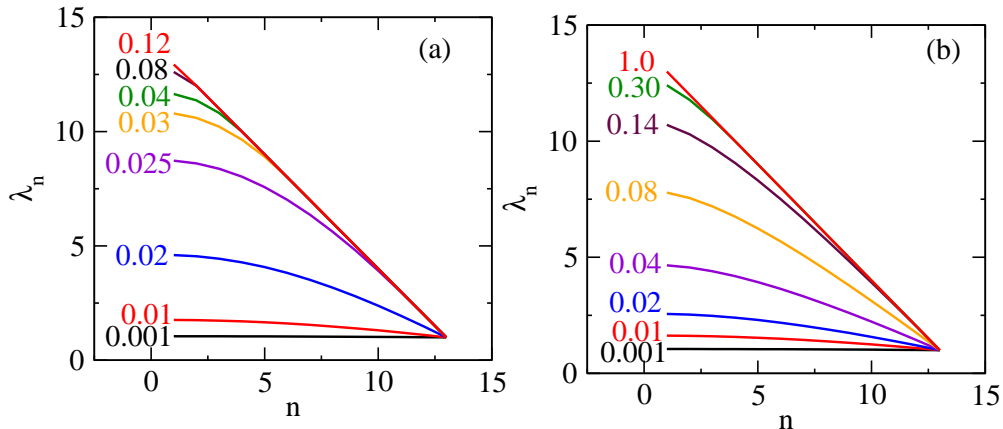


FIG. 5. Steady state stretch in different backbone segments in extensional flow at the indicated rates for a 27 arm comb mode with $\tau_a = 0.07$ s, $\tau_{seg,0} = 0.6$ s, and $\tau_o = 10^3$ s. The index increases from the central segments towards outside of the comb molecule. The plot on the left is predictions without drag-strain coupling (Eqn. 6) and the plot on the right is including drag-strain coupling (Eqn. 8) in the stretch evolution equations.

Overall, the agreement between model predictions and experiment, and the self-consistency of the model parameters, are encouraging. So, it would seem to be a meaningful exercise

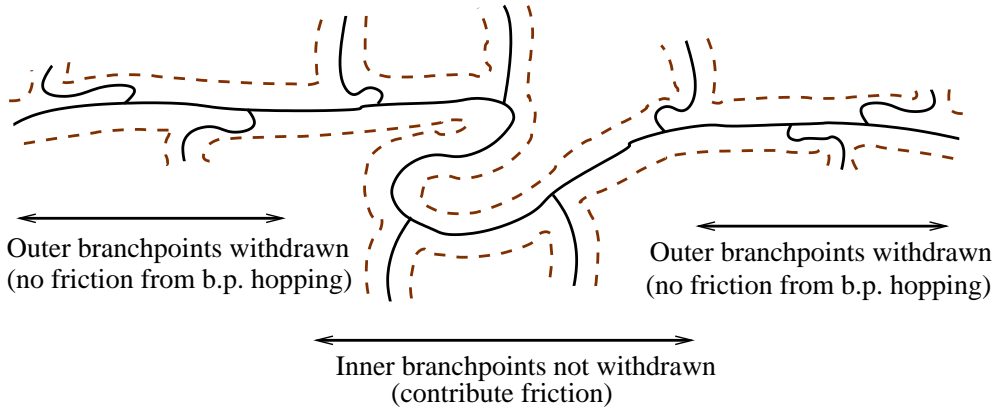


FIG. 6. Schematic representation of branch withdrawals in extensional flow (flow direction along the arrows).

to examine the internal dynamics of the stretch variables within the comb-model during start-up flow. We investigated the stretch dynamics in detail for a 27 arm comb mode with $\tau_a = 0.07$ s, $\tau_{seg,0} = 0.6$ s and $\tau_o = 10^3$ s. Fig. 5 shows the *steady state* stretch in different parts of the backbone for a range of extension rates; during start-up extensional flow, the stretch increases until it reaches this steady state value. So, in some sense, the curves in Fig. 5 represent a flow-rate-dependent priority for the backbone segments, i.e. a maximum value for the stretch which depends upon the flow rate, as suggested previously [Read *et al.*, 2011]. Towards the outside of the molecule it is clear that the maximal stretch is set by the branchpoint withdrawal limit; at higher rates the outermost segment has a stretch of 1, the next one in a stretch of 2, the next a stretch of 3, such that there is a linear envelope to the maximum stretch. This linear envelope to the maximum stretch was previously suggested for comb polymers by [Marrucci *et al.*, 2008]. However, there is an additional subtlety in our model. Once the outermost branchpoints are withdrawn, they no longer contribute friction to the remaining stretch dynamics in Eqns. 6 and 8. Thus, the effective friction is confined to the remaining central part of the molecule, comprising segments with non-withdrawn branchpoints; this section has a progressively faster relaxation time as more of the outer branchpoints are withdrawn. This situation is depicted schematically in Fig. 6, in which the outermost branches are in the withdrawn configuration, whilst the only friction arises from the hopping on the non-withdrawn inner branches. As a result, at intermediate flow rates, a steady state is reached in which stretching due to the flow is balanced by relaxation of this central section of the backbone. At these intermediate rates, although the center of

the comb initially begins to stretch strongly during the flow start-up, it does not reach the maximum stretch implied by the simple linear envelope obtained at higher flow rates.

In the absence of drag-strain coupling (Fig. 5a), this region of intermediate flow rates is quite narrow. Increasing the rate from 0.01 /s to 0.03 /s results in a transition from nearly unstretched to almost fully stretched conformation. With typical experimental measurements at rates separated by a factor of 3, it predicts a sharp critical value of strain rate above which nearly unstretched molecules reach their maximum stretch (except for the very center of the molecule). Drag-strain coupling (Fig. 5b) smooths this transition significantly. Fig 7 shows the steady-state stretch in the central segment as a function of the extension rate. With drag-strain coupling there is about a decade of $\dot{\epsilon}$ in which a concept of flow-rate dependent priority [Read *et al.*, 2011] is valid for the central segment. The range of validity of such a picture is much lower for the outerlying segments.

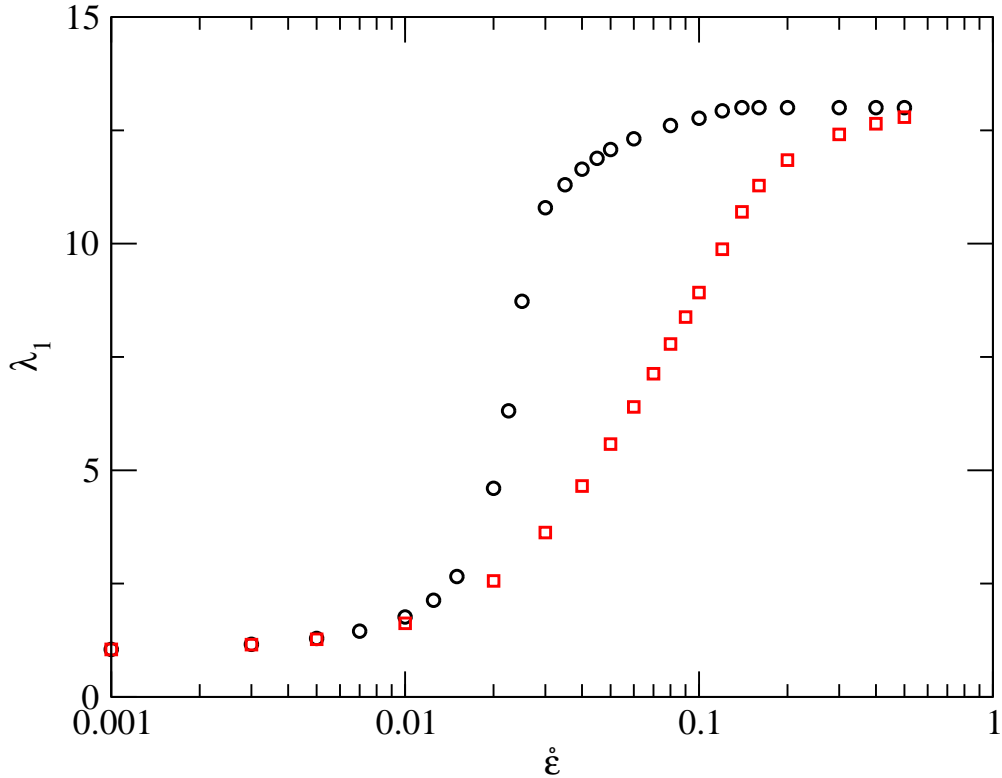


FIG. 7. Steady state stretch in the central segment for the comb molecule considered in Fig. 5 as a function of extension rate $\dot{\epsilon}$. Without drag-strain coupling (circles), there is a very short range of $\dot{\epsilon}$ in which the segment reaches its maximum stretch from essentially unstretched conformation. Drag-strain coupling (squares) smooth out this transition to some extent.

IV. CONCLUSIONS

We have presented a simple model, based on an extension to the pom-pom model, that captures the coupled stretch dynamics in a comb polymer under nonlinear flow (uniaxial extension). We use this self-consistent model to match, successfully, extensional data for a series of polystyrene and polyisoprene combs. Our strategy is to match the linear rheology of the resins with a Maxwell mode spectrum, and then to treat each of these Maxwell modes as either a non-stretching mode or as a comb mode. We use the side-arm retraction time τ_a to divide the modes in this way. Since the experimental extension rates were typically are much slower than τ_a ($\dot{\epsilon}\tau_a \ll 1$), reassigning a few additional modes as non-stretching mode does not significantly alter our predictions. Matching the extensional data requires a single fit parameter $\tau_{seg,0}$ for stretch diffusion in the backbone. We also demonstrate that our fitted values for this are physically reasonable (in the context of branchpoint hopping dynamics) across all the resins considered.

By examining, in detail, the stretch dynamics for a single mode of the model (Fig. 7), we conclude that the model is consistent with the concept of flow-dependent priority [Read *et al.*, 2011; Das *et al.*, 2014]. However, the local criteria for stretch dynamics implemented in [Read *et al.*, 2011; Das *et al.*, 2014] rested on the assumption that for highly polydisperse, randomly branched resins there is a wide distribution of relaxation times for side-arms. In the present (comb) case, all side arms are essentially the same length and have the same relaxation time. The result is that the dynamics of stretch relaxation along the backbone is more collective, with several branchpoints contributing to the modes of stretch relaxation. Predictions from the numerical algorithm of [Read *et al.*, 2011; Das *et al.*, 2014] fail to capture the sharp onset of strain hardening with the extension rate that is observed in the experimental data for these monodisperse combs. It might be that further refinements to that scheme, allowing for collective modes of stretch relaxation, would be able to capture the present comb data whilst improving the predictions for more polydisperse resins having both segment and architecture polydispersity.

ACKNOWLEDGEMENTS

We gratefully acknowledge support from the EU (FP7 ITN DYNACOP grant 214627).

APPENDIX: RESOLVING SMALL AMPLITUDE OSCILLATORY SHEAR DATA IN MAXWELL MODES

We resolve the experimental small amplitude oscillatory shear (SAOS) data to n_M Maxwell modes with the α -th mode having weight g_α and (given) relaxation time τ_α by minimizing the cost function

$$\mathcal{Q} \equiv \sum_{\omega} \left\{ \left(G'(\omega) - \sum_{\alpha} g_{\alpha} \frac{\omega^2 \tau_{\alpha}^2}{1 + \omega^2 \tau_{\alpha}^2} \right)^2 + \left(G''(\omega) - \sum_{\alpha} g_{\alpha} \frac{\omega \tau_{\alpha}}{1 + \omega^2 \tau_{\alpha}^2} \right)^2 \right\} - \lambda \sum_{\alpha} g_{\alpha}^2, \quad (\text{A1})$$

with respect to the set of g_{α} . Here $G'(\omega)$ and $G''(\omega)$ are the elastic and viscous modulus measured in SAOS at angular frequency ω . We have included an extra quadratic term in the weights g_{α} with a positive prefactor λ in \mathcal{Q} to ensure that all the weights are positive.

Variation with respect to g_{β} gives

$$\sum_{\alpha} a_{\alpha,\beta} g_{\alpha} - b_{\beta} = 0, \quad (\text{A2})$$

with

$$\begin{aligned} a_{\alpha,\beta} &= \sum_{\omega} \left\{ \frac{\omega^2 \tau_{\alpha} \tau_{\beta}}{(1 + \omega^2 \tau_{\alpha}^2)(1 + \omega^2 \tau_{\beta}^2)} [\omega^2 \tau_{\alpha} \tau_{\beta} + 1] \right\} - \lambda \delta_{\alpha,\beta}, \\ b_{\beta} &= \sum_{\omega} \left\{ G'(\omega) \frac{\omega^2 \tau_{\beta}^2}{1 + \omega^2 \tau_{\beta}^2} + G''(\omega) \frac{\omega \tau_{\beta}}{1 + \omega^2 \tau_{\beta}^2} \right\} \end{aligned} \quad (\text{A3})$$

To fit SAOS response between a maximum angular frequency ω_{max} and a minimum angular frequency ω_{min} , we set n_M to be 3 times the number of decades between ω_{min} and ω_{max} . We choose τ_M as equally distributed in log-scale between $1/\omega_{max}$ and $1/\omega_{min}$. Starting from a small $\lambda = 10^{-6}$, we solve the matrix equation A2 via Gauss-Jordan elimination with full pivoting. If any of the g_{α} were found to be negative, we increase λ by a factor 1.1 till all g_{α} are positive. This procedure also leads to reasonably smooth variation of g_M with τ_M .

The highest frequency experimental data was found to be harder to fit with Maxwell modes (which is not surprising given that the longitudinal Rouse modes can not be viewed as exponentially decaying modes). We limit our fitting procedure at frequencies below the high frequency cross-over of G' and G'' . We can fit the high frequency data at the expense of introducing extra oscillation in recalculated moduli from the set of computed Maxwell modes. In either case, the response from such high frequencies do not affect the start-up extensional response in which we use the Maxwell modes.

The Maxwell modes used for the resins are provided in tables A1 and A2. The SAOS data (symbols) and recalculated result using the Maxwell modes for PS742 are shown in Fig A1. Fig A2 shows a plot of the weights g_M as a function of times τ_M for PS742. For PS742, the final λ used in Eq. A2 was 0.1 and average deviation of recalculated moduli from the experimental data were within 5%. These numbers are representative for all the resins. Our choice of regularly (and densely) spaced τ_α stems from our use of these times as the separator between the stretching and the non-stretching modes. Note that there are a number of studies that have approached this inversion problem in a much more rigorous fashion [Mead, 1994; Cho and Park, 2013; Takeh and Shanbhag, 2013]. However, for our present need the simple minimization scheme presented here describes the data with sufficient accuracy.

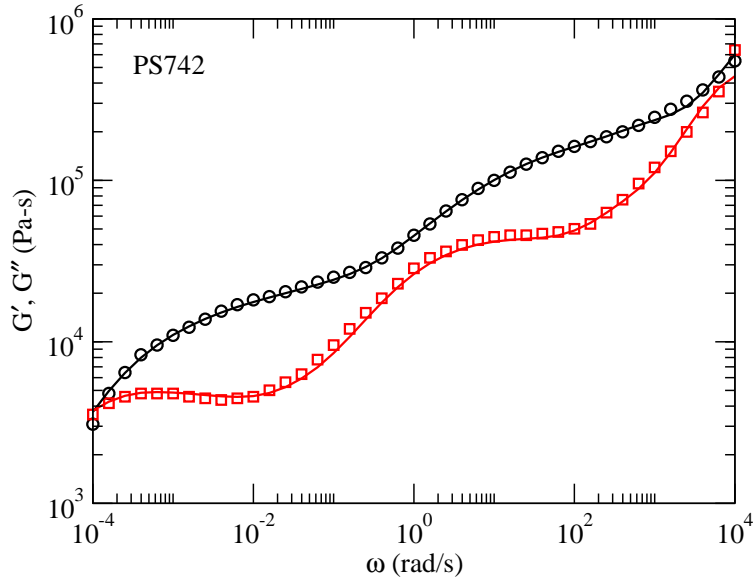


FIG. A1. Experimental SAOS response and calculated viscoelastic moduli from the Maxwell modes in table A2 for PS742.

| PI211 | | PI254 | | PI472 | | PS622 | | PS642 | |
|----------|---------|----------|---------|----------|---------|----------|---------|----------|---------|
| τ_M | g_M |
| (s) | (Pa) |
| 1.15e-5 | 1.06e+5 | 4.02e-6 | 3.54e+5 | 5.29e-6 | 1.84e+5 | 5.02e-5 | 9.17e+4 | 2.00e-5 | 2.06e+9 |
| 3.00e-5 | 2.25e+5 | 9.95e-6 | 6.51e+5 | 1.27e-5 | 3.62e+5 | 1.30e-4 | 1.89e+5 | 5.14e-5 | 3.99e+9 |
| 7.84e-5 | 2.77e+5 | 2.46e-5 | 6.26e+5 | 3.07e-5 | 4.50e+5 | 3.34e-4 | 2.24e+5 | 1.32e-4 | 3.91e+9 |
| 2.05e-4 | 1.60e+5 | 6.09e-5 | 1.67e+5 | 7.39e-5 | 2.56e+5 | 8.63e-4 | 1.27e+5 | 3.40e-4 | 1.26e+9 |
| 5.34e-4 | 6.18e+4 | 1.51e-4 | 2.37e+4 | 1.78e-4 | 7.36e+4 | 2.23e-3 | 6.21e+4 | 8.73e-4 | 1.63e+8 |
| 1.39e-3 | 4.21e+4 | 3.72e-4 | 5.56e+4 | 4.29e-4 | 3.79e+4 | 5.74e-3 | 4.39e+4 | 2.24e-3 | 2.36e+8 |
| 3.64e-3 | 4.64e+4 | 9.21e-4 | 4.83e+4 | 1.03e-3 | 5.18e+4 | 1.48e-2 | 3.03e+4 | 5.77e-3 | 2.62e+8 |
| 9.50e-3 | 3.47e+4 | 2.28e-3 | 2.97e+4 | 2.49e-3 | 5.05e+4 | 3.82e-2 | 1.71e+4 | 1.48e-2 | 3.09e+8 |
| 2.48e-2 | 2.00e+4 | 5.63e-3 | 3.45e+4 | 6.00e-3 | 3.30e+4 | 9.87e-2 | 1.01e+4 | 3.81e-2 | 3.88e+8 |
| 6.47e-2 | 1.78e+4 | 1.39e-2 | 4.56e+4 | 1.44e-2 | 1.73e+4 | 2.55e-1 | 7.66e+3 | 9.79e-2 | 3.87e+8 |
| 1.69e-1 | 2.10e+4 | 3.45e-2 | 4.88e+4 | 3.48e-2 | 1.01e+4 | 6.57e-1 | 6.90e+3 | 2.52e-1 | 3.20e+8 |
| 4.41e-1 | 2.26e+4 | 8.52e-2 | 4.43e+4 | 8.39e-2 | 8.54e+3 | 1.69e+0 | 7.07e+3 | 6.47e-1 | 2.07e+8 |
| 1.15e+0 | 2.46e+4 | 2.11e-1 | 3.76e+4 | 2.02e-1 | 8.97e+3 | 4.37e+0 | 7.74e+3 | 1.66e+0 | 8.91e+7 |
| 3.00e+0 | 2.81e+4 | 5.21e-1 | 3.17e+4 | 4.87e-1 | 1.06e+4 | 1.13e+1 | 7.35e+3 | 4.27e+0 | 3.23e+7 |
| 7.83e+0 | 3.40e+4 | 1.29e+0 | 2.13e+4 | 1.17e+0 | 1.25e+4 | 2.91e+1 | 4.55e+3 | 1.10e+1 | 2.14e+7 |
| 2.04e+1 | 3.96e+4 | 3.19e+0 | 1.40e+4 | 2.82e+0 | 1.38e+4 | 7.51e+1 | 1.25e+3 | 2.82e+1 | 1.85e+7 |
| 5.33e+1 | 3.57e+4 | 7.89e+0 | 1.15e+4 | 6.80e+0 | 1.50e+4 | 1.94e+2 | 6.15e+0 | 7.25e+1 | 1.52e+7 |
| 1.39e+2 | 2.02e+4 | 1.95e+1 | 1.01e+4 | 1.64e+1 | 1.72e+4 | 5.00e+2 | 1.58e+1 | 1.86e+2 | 1.11e+7 |
| 3.63e+2 | 5.43e+3 | 4.82e+1 | 9.15e+3 | 3.95e+1 | 1.97e+4 | – | – | 4.79e+2 | 4.04e+6 |
| 9.48e+2 | 2.22e+2 | 1.19e+2 | 9.40e+3 | 9.51e+1 | 2.24e+4 | – | – | 1.23e+3 | 8.76e+4 |
| 2.48e+3 | 1.60e+1 | 2.95e+2 | 9.54e+3 | 2.29e+2 | 2.76e+4 | – | – | 3.16e+3 | 3.50e+4 |
| – | – | 7.30e+2 | 6.51e+3 | 5.52e+2 | 3.48e+4 | – | – | – | – |
| – | – | 1.81e+3 | 2.34e+3 | 1.33e+3 | 3.59e+4 | – | – | – | – |
| – | – | 4.46e+3 | 2.85e+1 | 3.20e+3 | 2.55e+4 | – | – | – | – |
| – | – | – | – | 7.72e+3 | 1.08e+4 | – | – | – | – |
| – | – | – | – | 1.86e+4 | 2.50e+3 | – | – | – | – |
| – | – | – | – | 4.48e+4 | 1.03e+2 | – | – | – | – |

TABLE A1. Maxwell times and weights for PI211, PI254, PI472, PS622, and PS642.

| PS712 | | PS722 | | PS732 | | PS742 | |
|----------|---------|----------|---------|----------|---------|----------|---------|
| τ_M | g_M | τ_M | g_M | τ_M | g_M | τ_M | g_M |
| (s) | (Pa) | (s) | (Pa) | (s) | (Pa) | (s) | (Pa) |
| 2.00e-5 | 4.93e+5 | 2.00e-5 | 7.78e+4 | 2.00e-5 | 3.67e+5 | 2.00e-5 | 2.69e+5 |
| 4.73e-5 | 7.82e+5 | 5.12e-5 | 1.68e+5 | 4.83e-5 | 6.00e+5 | 5.12e-5 | 5.00e+5 |
| 1.12e-4 | 5.39e+5 | 1.31e-4 | 2.25e+5 | 1.16e-4 | 4.19e+5 | 1.31e-4 | 3.74e+5 |
| 2.65e-4 | 9.57e+3 | 3.36e-4 | 1.53e+5 | 2.81e-4 | 6.76e+3 | 3.36e-4 | 8.92e+3 |
| 6.26e-4 | 3.81e+4 | 8.62e-4 | 7.22e+4 | 6.78e-4 | 1.10e+4 | 8.62e-4 | 1.12e+4 |
| 1.48e-3 | 8.85e+4 | 2.21e-3 | 3.83e+4 | 1.64e-3 | 5.61e+4 | 2.21e-3 | 4.69e+4 |
| 3.50e-3 | 3.06e+4 | 5.66e-3 | 2.79e+4 | 3.95e-3 | 2.91e+4 | 5.66e-3 | 2.18e+4 |
| 8.28e-3 | 1.85e+4 | 1.45e-2 | 2.01e+4 | 9.52e-3 | 3.25e+4 | 1.45e-2 | 1.96e+4 |
| 1.96e-2 | 7.11e+3 | 3.71e-2 | 1.27e+4 | 2.30e-2 | 3.74e+4 | 3.71e-2 | 2.75e+4 |
| 4.63e-2 | 5.70e+3 | 9.52e-2 | 8.23e+3 | 5.54e-2 | 2.76e+4 | 9.52e-2 | 2.74e+4 |
| 1.09e-1 | 8.92e+3 | 2.44e-1 | 6.30e+3 | 1.34e-1 | 1.73e+4 | 2.44e-1 | 2.55e+4 |
| 2.59e-1 | 6.56e+3 | 6.25e-1 | 5.66e+3 | 3.23e-1 | 8.46e+3 | 6.25e-1 | 2.09e+4 |
| 6.12e-1 | 6.31e+3 | 1.60e+0 | 5.42e+3 | 7.79e-1 | 3.66e+3 | 1.60e+0 | 1.20e+4 |
| 1.45e+0 | 8.48e+3 | 4.10e+0 | 5.63e+3 | 1.88e+0 | 3.01e+3 | 4.10e+0 | 4.69e+3 |
| 3.42e+0 | 1.03e+4 | 1.05e+1 | 7.21e+3 | 4.53e+0 | 3.32e+3 | 1.05e+1 | 2.56e+3 |
| 8.10e+0 | 1.34e+4 | 2.69e+1 | 9.54e+3 | 1.09e+1 | 4.44e+3 | 2.69e+1 | 2.56e+3 |
| 1.92e+1 | 1.66e+4 | 6.90e+1 | 1.14e+4 | 2.64e+1 | 3.94e+3 | 6.90e+1 | 2.12e+3 |
| 4.53e+1 | 1.88e+4 | 1.77e+2 | 1.31e+4 | 6.37e+1 | 4.10e+3 | 1.77e+2 | 2.48e+3 |
| 1.07e+2 | 1.21e+4 | 4.53e+2 | 1.46e+4 | 1.54e+2 | 7.13e+3 | 4.53e+2 | 2.90e+3 |
| 2.53e+2 | 2.09e+4 | 1.16e+3 | 1.33e+4 | 3.71e+2 | 8.51e+3 | 1.16e+3 | 2.94e+3 |
| 5.99e+2 | 3.01e+4 | 2.97e+3 | 8.04e+3 | 8.94e+2 | 8.51e+3 | 2.97e+3 | 3.66e+3 |
| 1.42e+3 | 1.50e+4 | 7.62e+3 | 2.64e+3 | 2.16e+3 | 6.74e+3 | 7.62e+3 | 2.93e+3 |
| 3.35e+3 | 3.99e+3 | 1.95e+4 | 3.78e+2 | 5.21e+3 | 4.28e+3 | 1.95e+4 | 1.40e+3 |
| 7.92e+3 | 2.25e+3 | 5.00e+4 | 1.05e+1 | 1.26e+4 | 4.17e+3 | 5.00e+4 | 1.19e+3 |

TABLE A2. Maxwell times and weights for PS712, PS722, PS732, and PS742.

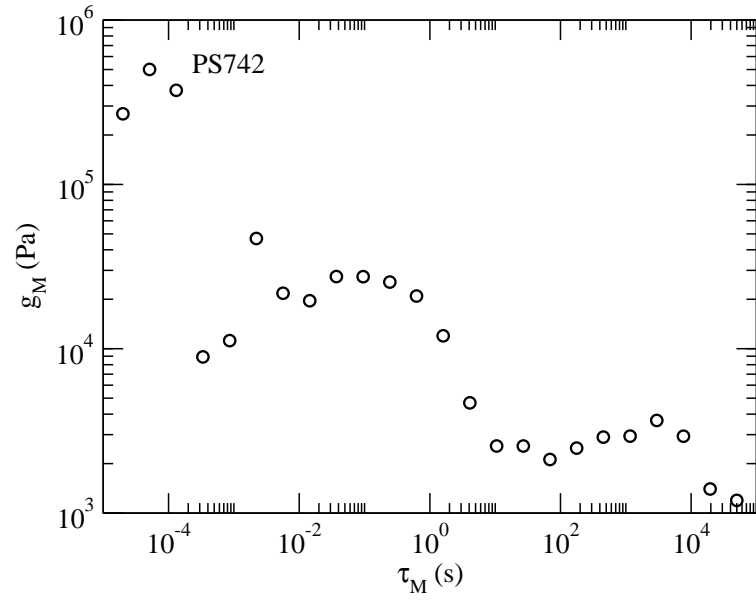


FIG. A2. The weights (g_M) of the fitted Maxwell modes as a function of relaxation times (τ_M) for PS742.

REFERENCES

- Ahmadi, M., Bailly, C., Keunings, R., Nekoomanesh, M., Arabi, H., and van Ruymbeke, E., “Time marching algorithm for predicting the linear rheology of monodisperse comb polymer melts,” *Macromolecules* **44**, 647–659 (2011).
- Báčová, P., Lentzakis, H., Read, D. J., Moreno, A. J., Vlassopoulos, D., and Das, C., “Branchpoint motion in architecturally complex polymers: estimation of hopping parameters from computer simulations and experiments,” *Macromolecules* **47**, 3362–3377 (2014).
- Ball, R. C. and McLeish, T. C. B., “Dynamic dilution and the viscosity of star polymer melts,” *Macromolecules* **22**, 1911–1913 (1989).
- Bick, D. K. and McLeish, T. C. B., “Topological contributions to nonlinear elasticity in branched polymers,” *Phys. Rev. Lett.* **76**, 2587–2590 (1996).
- Bird, R. B., Armstrong, R. C., and Hassager, O., *Dynamics of polymeric liquids. Volume 1: Fluid mechanics* (Wiley-Interscience, 1987).
- Blackwell, R. J., Harlen, O. G., and McLeish, T. C. B., “Theoretical linear and nonlinear rheology of symmetric treelike polymer melts,” *Macromolecules* **34**, 2579–2596 (2001).
- Blackwell, R. J., McLeish, T. C. B., and Harlen, O. G., “Molecular drag-strain coupling in branched polymer melts,” *J. Rheol.* **44**, 121–136 (2000).
- Chambon, P., Fernyhough, C. M., Im, K., Chang, T., Das, C., Embery, J., McLeish, T. C. B., and Read, Daniel, J., “Synthesis, temperature gradient interaction chromatography, and rheology of entangled styrene comb polymers,” *Macromolecules* **41**, 5869–5875 (2008).
- Chen, X., Shahinur Rahman, M., Lee, H., Mays, J., Chang, T., and Larson, R., “Combined synthesis, tgc characterization, and rheological measurement and prediction of symmetric h polybutadienes and their blends with linear and star-shaped polybutadienes,” *Macromolecules* **44**, 7799–7809 (2011).
- Cho, K. S. and Park, G. W., “Fixed-point iteration for relaxation spectrum from dynamic mechanical data,” *J. Rheol.* **57**, 647–678 (2013).
- Das, C., Inkson, N. J., Read, D. J., Kelmanson, M. A., and McLeish, T. C. B., “Computational linear rheology of general branch-on-branch polymers,” *J. Rheol.* **50**, 207–235 (2006a).
- Das, C., Read, D. J., Auhl, D., Kapnistos, M., den Doelder, J., Vittorias, I., and McLeish, T. C. B., “Numerical prediction of non-linear rheology of branched polymer melts,” *J.*

- Rheol. **58**, 737–757 (2014).
- Das, C., Read, D. J., Kelmanson, M. A., and McLeish, T. C. B., “Dynamic scaling in entangled mean-field gelation polymers,” *Phys. Rev. E* **74**, 011404 (2006b).
- Dealy, J. M. and Larson, R. G., *Structure and rheology of molten polymers: from structure to flow behavior and back again* (Hanser Verlag, 2006).
- Doi, M. and Edwards, S. F., *The theory of polymer dynamics* (Clarendon Press, Oxford, 1986).
- Fetters, L. J., Lohse, D. J., Richter, D., Witten, T. A., and Zirkel, A., “Connection between polymer molecular weight, density, chain dimensions, and melt viscoelastic properties,” *Macromolecules* **27**, 4639–4647 (1994).
- Hassell, D. G., Hoyle, D., Auhl, D., Harlen, O., Mackley, M. R., and McLeish, T. C. B., “Effect of branching in cross-slot flow: the formation of “w cusps”,” *Rheol Acta* **48**, 551–561 (2009).
- Hatzikiriakos, S. G., “Long chain branching and polydispersity effects on the rheological properties of polyethylenes,” *Polym. Eng. Sci.* **40**, 2279–2287 (2000).
- Hutchings, L. R., Kimani, S. M., Hoyle, D. M., Read, D. J., Das, C., McLeish, T. C. B., Chang, T., Lee, H., and Auhl, D., “In silico molecular design, synthesis, characterization, and rheology of dendritically branched polymers: closing the design loop,” *ACS Macro Letters* **1**, 404–408 (2012).
- Ianniruberto, G. and Marrucci, G., “Entangled melts of branched ps behave like linear ps in the steady state of fast elongational flows,” *Macromolecules* **46**, 267–275 (2012).
- Inkson, N. J., Graham, R. S., McLeish, T. C. B., Groves, D. J., and Fernyhough, C. M., “Viscoelasticity of monodisperse comb polymer melts,” *Macromolecules* **39**, 4217–4227 (2006).
- Inkson, N. J., McLeish, T. C. B., Harlen, O. G., and Groves, D. J., “Predicting low density polyethylene melt rheology in elongational and shear flows with “pom-pom” constitutive equations,” *J. Rheol.* **43**, 873–896 (1999).
- Kapnistos, M., Kirkwood, K. M., Ramirez, J., Vlassopoulos, D., and Leal, L. G., “Nonlinear rheology of model comb polymers,” *J. Rheol.* **53**, 1133–1153 (2009).
- Kapnistos, M., Vlassopoulos, D., Roovers, J., and Leal, L. G., “Linear rheology of architecturally complex macromolecules: Comb polymers with linear backbones,” *Macromolecules* **38**, 7852–7862 (2005).

- Kasehagen, L. J. and Macosko, C. W., “Nonlinear shear and extensional rheology of long-chain randomly branched polybutadiene,” *J. Rheol.* **42**, 1303–1327 (1998).
- Kirkwood, K. M., Leal, L. G., Vlassopoulos, D., Driva, P., and Hadjichristidis, N., “Stress relaxation of comb polymers with short branches,” *Macromolecules* **42**, 9592–9608 (2009).
- Larson, R. G., “Combinatorial rheology of branched polymer melts,” *Macromolecules* **34**, 4556–4571 (2001).
- Larson, R. G., Zhou, Q., Shanbhag, S., and Park, S. J., “Advances in modeling of polymer melt rheology,” *AIChE J.* **53**, 542–548 (2007).
- Lentzakis, H., Vlassopoulos, D., Read, D. J., Lee, H., T., C., Driva, P., and Hadjichristidis, N., “Uniaxial extensional rheology of well-characterized comb polymers,” *J. Rheol.* **57**, 605–625 (2013).
- Li, S. W., Park, H. E., Dealy, J. M., Maric, M., Lee, H., Im, K., Choi, H., Chang, T., Shahinur Rahman, M., and Mays, J., “Detecting structural polydispersity in branched polybutadienes,” *Macromolecules* **44**, 208–214 (2010).
- Marrucci, G., Ianniruberto, G., Bacchelli, F., and Coppola, S., “Unusual nonlinear effects in the rheology of entangled polymer melts,” *Prog. Theo. Phys. Sup.* **175**, 1–9 (2008).
- McLeish, T., “A tangled tale of topological fluids,” *Physics today.* **61**, 40–45 (2008).
- McLeish, T. C. B., “Tube theory of entangled polymer dynamics,” *Adv. Phys.* **52**, 1379–1527 (2002).
- McLeish, T. C. B. and Larson, R. G., “Molecular constitutive equations for a class of branched polymers: The pom-pom polymer,” *J. Rheol.* **42**, 81–110 (1998).
- Mead, D. W., “Numerical interconversion of linear viscoelastic material functions,” *J. Rheol.* **38**, 1769–1795 (1994).
- Mendelson, R. A., Bowles, W. A., and Finger, F. L., “Effect of molecular structure on polyethylene melt rheology. ii. shear-dependent viscosity,” *J. Polym. Sci. A-2* **8**, 127–141 (1970).
- Milner, S. T. and McLeish, T. C. B., “Parameter-free theory for stress relaxation in star polymer melts,” *Macromolecules* **30**, 2159–2166 (1997).
- Nielsen, J. K., Rasmussen, H. K., Denberg, M., Almdal, K., and Hassager, O., “Nonlinear branch-point dynamics of multiarm polystyrene,” *Macromolecules* **39**, 8844–8853 (2006).
- Press, W. H., Teukolsky, S. A., Vetterling, W. T., and Flannery, B. P., *Numerical recipes in C++: The art of scientific computing*, 2nd ed. (Cambridge University Press, 1992).

- Read, D. J., Auhl, D., Das, C., den Doelder, J., Kapnistos, M., Vittorias, I., and McLeish, T. C. B., “Linking models of polymerization and dynamics to predict branched polymer structure and flow,” *Science* **333**, 1871–1874 (2011).
- Read, D. J. and McLeish, T. C. B., “Molecular rheology and statistics of long chain branched metallocene-catalyzed polyolefins,” *Macromolecules* **34**, 1928–1945 (2001).
- Rolón-Garrido, V. H., Pivokonsky, R., Filip, P., Zatloukal, M., and Wagner, M. H., “Modelling elongational and shear rheology of two ldpe melts,” *Rheo. acta* **48**, 691–697 (2009).
- Roovers, J., “Synthesis and dilute solution characterization of comb polystyrenes,” *Polymer* **20**, 843–849 (1979).
- Roovers, J. and Graessley, W. W., “Melt rheology of some model comb polystyrenes,” *Macromolecules* **14**, 766–773 (1981).
- van Ruymbeke, E., Kapnistos, M., Vlassopoulos, D., Huang, T., and Knauss, D. M., “Linear melt rheology of pom-pom polystyrenes with unentangled branches,” *Macromolecules* **40**, 1713–1719 (2007).
- Samurkas, T., Dealy, J. M., and Larson, R. G., “Strong extensional and shearing flows of a branched polyethylene,” *J. Rheol.* **33**, 559–578 (1989).
- Sentmanat, M. L., “Miniature universal testing platform: from extensional melt rheology to solid-state deformation behavior,” *Rheo. Acta* **43**, 657–669 (2004).
- Snijkers, F., van Ruymbeke, E., Kim, P., Lee, H., Nikopoulou, A., Chang, T., Hadjichristidis, N., Pathak, J., and Vlassopoulos, D., “Architectural dispersity in model branched polymers: Analysis and rheological consequences,” *Macromolecules* **44**, 8631–8643 (2011).
- Snijkers, F., Vlassopoulos, D., Ianniruberto, G., Marrucci, G., Lee, H., Yang, J., and Chang, T., “Double stress overshoot in start-up of simple shear flow of entangled comb polymers,” *Macro Letters* **2**, 601–604 (2013).
- Takeh, A. and Shanbhag, S., “A computer program to extract the continuous and discrete relaxation spectra from dynamic viscoelastic measurements,” *Appl. Rheol.* **23**, 24628 (2013).
- Van Ruymbeke, E., Muliawan, E. B., Hatzikiriakos, S. G., Watanabe, T., Hirao, A., and Vlassopoulos, D., “Viscoelasticity and extensional rheology of model cayley-tree polymers of different generations,” *J. Rheol.* **54**, 643–662 (2010).
- Wagner, Manfred, H. and Rolón-Garrido, V. H., “Verification of branch point withdrawal in elongational flow of pom-pom polystyrene melt,” *J. Rheol.* **52**, 1049–1068 (2008).
- Wood-Adams, P. M., Dealy, J. M., deGroot, W. A., and Redwine, D. O., “Effect of molecular

structure on the linear viscoelastic behavior of polyethylene,” *Macromolecules* **33**, 7489–7499 (2000).

Zhou, Q. and Larson, R. G., “Direct molecular dynamics simulation of branch point motion in asymmetric star polymer melts,” *Macromolecules* **40**, 3443–3449 (2007).